energy&fuels

Article

Cite This: *Energy Fuels* 2018, 32, 9106−9120

pubs.acs.org/EF

Advances in Asphaltene Petroleomics. Part 3. Dominance of Island or Archipelago Structural Motif Is Sample Dependent

Martha L. Chacón-Patiño,[†] Steven M. Rowland,[†,‡] and Ryan P. Rodgers*[,†,‡,§]

[†]National High Magnetic Field Laboratory, Florida State University, Tallahassee, Florida 32310, United States

[‡]Future Fuels Institute, Florida State University, 1800 East Paul Dirac Drive, Tallahassee, Florida 32310, United States

[§]Department of Chemistry and Biochemistry, Florida State University, 95 Chieftain Way, Tallahassee, Florida 32306, United States

Supporting Information

ABSTRACT: Asphaltene structure is one of the most controversial topics in petroleum chemistry. The controversy is centered on the organization of aromatic cores within asphaltene molecules (single aromatic core, island and multiple aromatic core, archipelago) and specifically the inconsistency between the *island* model and the composition of the products derived from asphaltene pyrolysis/thermal cracking. Such products are consistent with the coexistence of *island* and *archipelago* asphaltene structural motifs. However, the archipelago model continues to lack the widespread acceptance of the petroleum community, in part due to mass spectrometry results in support of the island model. In the first and second part of this series, we demonstrated that the disproportionally high atmospheric pressure photoionization (APPI) ionization efficiency (monomer ion yield) of island species is due to weak nanoaggregation of large aromatic cores which do not extensively aggregate in toluene, whereas more archipelago-dominant fractions were shown to have low monomer ion yield due to a greater propensity for aggregation. The discrepancy leads to bias toward the selective ionization of island compounds and thus the erroneous mass spectrometry support of the predominance of the island structural model. A separation method based on aggregation trends and therefore the efficiency of monomeric ion production is critical to access archipelago structures. In the work presented herein, we demonstrate that dominance of island or archipelago structural motif is sample dependent. We present the positive-ion APPI Fourier transform ion cyclotron resonance mass spectrometry (FT-ICR MS) characterization of asphaltenes and asphaltene extrography fractions derived from Wyoming Deposit (island dominant) and Athabasca Bitumen (archipelago dominant) C_7 asphaltenes. Wyoming Deposit asphaltenes resemble the "classical" island-type asphaltene structure: they exhibit a high concentration of highly aromatic/alkyl-deficient species with a compositional space close to the polycyclic aromatic hydrocarbon (PAH) limit. Fragmentation results from infrared multiphoton dissociation (IRMPD) confirm that island is the dominant structural motif in Wyoming Deposit C_7 asphaltenes; the predominant fragmentation pathway for all extrography fractions consists of loss of CH_2 units (or dealkylation), without significant loss of aromaticity. Conversely, Athabasca Bitumen C_7 asphaltenes exhibit an "atypical" molecular composition. More than 40 wt % of the sample is extracted in the latest extrography fractions, which are composed of difficult-to-ionize species, a fraction of which exhibit atypically low double bond equivalent (DBE = 5−12) and extended homologous series with carbon numbers up to 60. The fragmentation behavior of all Athabasca Bitumen-derived fractions demonstrates a predominant contribution of archipelago motifs. Our results suggest that the Yen-Mullins molecular definition of asphaltenes cannot be used to describe all asphaltene samples. Island and archipelago structural motifs coexist, and extrography separation reveals a structural continuum that is enriched with archipelago motifs as a function of increasing molecular weight and polarity. The ratio island/archipelago is sample dependent, and its accurate quantification should significantly improve the economic value of asphaltene-enriched feedstocks by prediction of yields and optimal conditions for upgrading processes.

INTRODUCTION

Asphaltenes are well known for their negative impact on petroleum production,[1−4] transportation,[5−7] refining,[8,9] and storage.[10] Although these compounds are one of the most problematic and widely studied chemical classes in the petroleum industry, little consensus exists in their structure and composition. Such information is crucial, as an accurate knowledge of asphaltene chemistry and structure should lead to the rational design of methods to solve asphaltene-related problems and maximize the yield of valuable products from heavy feedstocks.[9,11] However, asphaltene structure is one of the most controversial topics in petroleum chemistry, and the nature of the organization of aromatic cores within asphaltene molecules has been the subject of intense and continuous debates.[12−17]

Traditionally, asphaltenes are described as compounds consisting of a single aromatic core of approximately seven fused rings, with alkyl side chains and N-, O-, and S-containing functionalities.[13,18,19] This structural model, termed island, is widely supported by X-ray diffraction (XRD),[20,21] time-resolved fluorescence depolarization (TRFD),[13] atomic force microscopy (AFM),[22,23] and mass spectrometry (MS).[24−26] In particular, results derived from tandem MS have strengthened

Received: May 22, 2018
Revised: August 14, 2018
Published: August 28, 2018

DOI: 10.1021/acs.energyfuels.8b01765
Energy Fuels 2018, 32, 9106−9120

the general (but incorrect) hypothesis that regardless of geological origin, the dominant structure in all asphaltene samples is island. However, controversy on the universal dominance of island structures persists because it is impossible to reconcile asphaltene bulk properties (especially pyrolysis and thermal cracking products) with the island model.[27−32] Such observations support the archipelago model, which proposes that asphaltene molecules have several aromatic cores linked by covalent bridges.[15,33,34] However, the archipelago model is not as widely accepted by the petroleum comunity; according to several publications, it is inconsistent with XRD, TRFD, AFM, and MS results.[13,20−25,35−39]

In mild pyrolysis and thermal cracking, petroleum asphaltenes yield coke (toluene insoluble), residual asphaltenes (toluene soluble and heptane insoluble), naphtha-range alkanes, distillable alkyl-aromatics (soluble in toluene and heptane), and gas.[30,40,41] Moreover, asphaltene samples from different geological origin yield different ratios of coke/distillable products.[29,33,42−44] Given that island-type species preferentially yield coke, naphtha-range alkanes, and gas,whereas archipelago-type compounds produce 1−5 ring alkyl-aromatics, asphaltene samples should be mixtures of island and archipelago motifs.[45] Most importantly, the crude oil dependence of these yields strongly suggests that the ratio island/archipelago must be sample dependent.[46]

Archipelago Motifs Are Elusive. In the first and second part of the series *Advances in Asphaltene Petroleomics*, it was demonstrated that petroleum asphaltenes are ultracomplex mixtures of abundant island and archipelago motifs.[46,47] We revealed the reason behind the mass spectral support of the island model is rooted in the preferential ionization of island structures,[46] as it is well known that heterogeneous aggregation of asphaltenes imparts a limitation on complete characterization by MS.[15,48] Simply, specific asphaltene fractions exhibit a disproportionally high tendency for aggregation,[49,50] which decreases the signal of monomeric ions in mass spectrometry.[47] Thus, *monomer ion yield* (MIY), a value inversely proportional to the accumulation period required to detect a target signal magnitude, was defined to sort asphaltene samples based on their production efficiency of monomeric ions. An extrography method was then developed to separate asphaltenes into fractions with similar MIY. In this method, the fractionation is performed by two solvent series: the first consists of acetone and acetonitrile and targets the selective removal of asphaltene species that exhibit high MIY and thus restrict complete MS characterization. The second series uses heptane, toluene, tetrahydrofuran, and methanol to separate remnant asphaltenes based on polarity. Results on the interlaboratory sample known as *Petrophase 2017* and South American Medium asphaltenes demonstrate that the acetone fraction, with the highest MIY, resembles the molecular composition of the parent, unfractionated asphaltene sample and yields IRMPD fragments that reveal abundant island structures.[47] The selective removal of compounds with high MIY facilitates the observation of otherwise undetected species. The latest eluting fractions exhibit poor ionization efficiency in APPI but reveal IRMPD fragment ions only possible for archipelago structures. Aggregation tests suggest that MIY decreases as a function of increasing aggregation tendency in Hep/Tol. Therefore, APPI MS analyses of unfractionated samples fail to reveal archipelago species due to the preferential ionization of highly aromatic/alkyl-deficient, nonaggregated island structures, not because of their absence.[47] In other words, separation of asphaltenes based on aggregation (into fractions of similar ionization efficiency) is critical for a more complete structural and compositional characterization by MS.

In addition to the intrinsic bias imparted by the preferential ionization of island structures in APPI, the efficiency of the fragmentation is also crucial to detect archipelago structures. IRMPD and collision-induced dissociation (CID) are two of the most widely used fragmentation techniques. IRMPD of model compounds yields the most stable aromatic building blocks by efficient fragmentation of alkyl side chains and covalent bridges between aromatic cores.[16,46] However, this is not always the case for collision-induced dissociation (CID). Nyadong et al.[51] demonstrated that low-energy CID, commonly employed to support the dominance of island motifs in coal/petroleum asphaltenes,[37,52−54] does not provide the energy required to fragment archipelago molecules composed of multiple aromatic cores. Conversely, high-energy collision-induced dissociation (HCD) was shown to be much more suitable for the complete fragmentation of model structures into their stable aromatic cores, which facilitates elucidation of island and archipelago motifs by changes in DBE after dissociation.[51] In another report, Kenttämaa et al.[55] demonstrated that CID produces incomplete fragmentation of island and archipelago model structures and thus suggested the use of higher energy, beam-type collision-activated dissociation (beam CAD) to access archipelago motifs in model compounds and petroleum samples.

The elusiveness of archipelago structural motifs is not limited to mass spectrometry. Ruiz-Morales et al.[56] reported a theoretical approach, through molecular orbital calculations, to understand the stability and size of asphaltene dimers composed of island and archipelago structures. Ruiz-Morales concluded that TRFD could detect species composed of two aromatic cores liked by an aryl−aryl bridge (archipelago)[23] as island compounds; thus, to some extent, TRFD blurs the discrimination between island and archipelago.[56] Furthermore, the access to archipelago structures via AFM appears to be troublesome as compared to island species. Admittedly, Schuler et al.[39] recognized that AFM is more powerful on planar molecules (island) and demonstrated that detection of archipelago motifs required inducing a planar conformation in the saturated bridges.[39] Moreover, it is essential to bear in mind that AFM requires unique sample preparation, in which asphaltenes (known to concentrate in "nondistillable" petroleum residues) must be sublimated and subsequently deposited onto a surface.[23] Interestingly, most of the reported structures for UG-8 Kuwait asphaltenes consist of highly aromatic/alkyl-deficient compounds, which exhibit H/C ratios between $0.41 < H/C < 0.60$, much lower than the accepted bulk H/C ratio of ∼1.05.[23,57]

Correlating Bulk Behavior with Asphaltene Structure. Molecular structure determines properties and reactivity. Therefore, the dominant structure in Athabasca Bitumen is hypothetically archipelago,[45,58−60] as Strausz et al. found that under mild conditions, thermolysis of Athabasca Bitumen asphaltenes yields an extensive amount of alkyl-substituted 1−5 ring aromatics.[12,61] Similarly, flash pyrolysis of this asphaltene sample can produce pyrolysis oils in yields up to 37 wt %, with a maltene fraction composed of abundant alkyl-substituted benzo- and dibenzothiophenes.[61] Strausz et al.[12] also reported the use of ruthenium-ion-catalyzed oxidation (RICO) for structural elucidation of asphaltenes from diverse geological origin. RICO targets the selective oxidation of aromatic moieties. Thus, alkyl-substituted aromatic cores are converted to CO;

DOI: 10.1021/acs.energyfuels.8b01765
Energy Fuels 2018, 32, 9106−9120

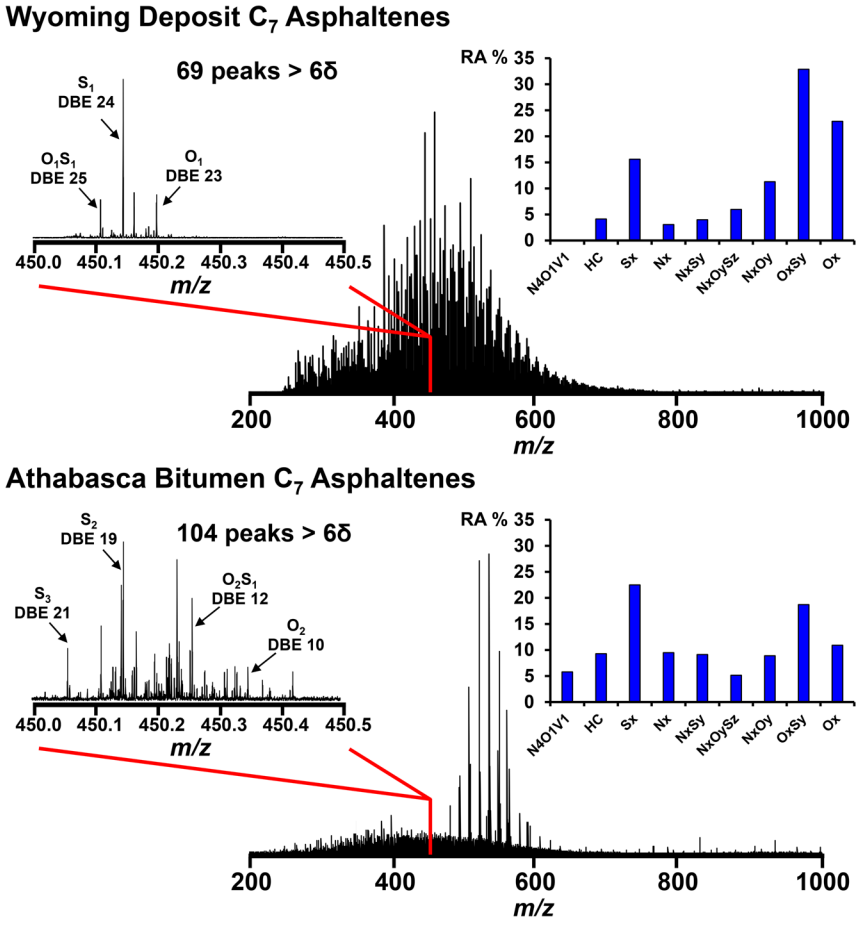

Figure 1. Positive-ion APPI FT-ICR MS mass spectra with zoomed mass insets at m/z 450 and heteroatom group distributions for (top) Wyoming Deposit C_7 asphaltenes and (bottom) Athabasca Bitumen C_7 asphaltenes.

however, carbons with alkyl substitution survive and are converted to a carboxylic acid linked to the initial alkyl group. Strausz et al.[12] attributed the high production of dialkanoic acids to a high abundance of archipelago motifs in Athabasca Bitumen asphaltenes.[12]

In another work, Rueda-Velásquez et al.[41] and Juyal et al.[62] studied the thermal cracking behavior of C_7 asphaltenes derived from Wyoming Deposit and Athabasca Bitumen. Under the same conditions, Wyoming Deposit asphaltenes yield ~30.4 wt % of coke and only 24.5 wt % of distillable products, whereas Athabasca Bitumen asphaltenes produce ~57.4 wt % of distillates and ~5.0 wt % coke. The authors concluded that the yields of distillable products and coke for Wyoming Deposit asphaltenes are consistent with a high concentration of large/alkyl-deficient island-type aromatics. Conversely, the characterization of distillable products from Athabasca Bitumen asphaltenes by gas chromatography-MS demonstrated a high concentration of 1−4 ring alkyl-aromatics and alkyl-substituted benzo- and dibenzothiophenes. These building blocks are consistent with abundant archipelago structural motifs.

The work presented herein focuses on a comprehensive study of the structure and composition of Wyoming Deposit and Athabasca Bitumen C_7 asphaltenes by an extrography fractionation method to separate asphaltene samples on the basis of aggregation trends and, therefore, monomer ion yield. Whole samples and fractions are characterized by positive-ion APPI FT-ICR MS, and fragmentation was performed by IRMPD. Our results demonstrate that island is the dominant structure for Wyoming Deposit asphaltenes; these species fit into the classical molecular definition that describes asphaltenes as alkyl-deficient/single-core aromatic compounds with high stability in fragmentation due to their increased aromatic condensation. In contrast, Athabasca bitumen asphaltenes exhibit atypically low aromaticity, a high degree of alkyl substitution, and a fragmentation behavior consistent with abundant archipelago motifs. We demonstrate that the island-dominant molecular definition of asphaltenes does not describe all asphaltene samples. The dominance of island or archipelago is shown to be sample dependent, and thus, the quantification of each motif should provide an accurate methodology to predict yields and conditions for upgrading of asphaltene-enriched feedstocks (process-dependent economic value).

EXPERIMENTAL SECTION

Materials. High-performance liquid chromatography (HPLC)-grade dichloromethane (DCM), *n*-heptane (C_7 or Hep), acetone, acetonitrile (ACN), toluene (Tol), tetrahydrofuran (THF), methanol (MeOH), and high-purity grade chromatographic silica gel (70−230 mesh, pore size 60 Å, Fluka Analytical) were used as received. Whatman filter paper grade 42 and high-purity glass microfiber thimbles were used for asphaltene isolation and Soxhlet extraction (Whatman, GE Healthcare, Little Chalfont, U.K.). Samples of the Wyoming Deposit were supplied by Nalco Champion; Athabasca Bitumen samples were supplied by the National Center for Upgrading Technology (NCUT).

Asphaltene Precipitation and Fractionation. Asphaltenes were isolated from Wyoming Deposit and Athabasca Bitumen by a modified version of the standard ASTM method D6560-12 published else-

DOI: 10.1021/acs.energyfuels.8b01765
Energy Fuels 2018, 32, 9106−9120

where.[63] Briefly, 400 mL of C_7 was added dropwise to 10 g of Wyoming Deposit and Athabasca Bitumen samples under sonication (Branson Ultrasonics, Danbury, CT, 22 kHz, and 130 W) at ~75 °C. The mixtures were refluxed at ~110 °C for 1 h and allowed to stand overnight. The precipitated solids were collected by filtration and washed with C_7 in a Soxhlet apparatus until the solvent appeared colorless. Asphaltenes were recovered by dissolution in hot toluene and dried under N_2 flow. Further purification of asphaltenes was performed as reported by Chacón-Patiño et al.[63] In short, solid C_7 asphaltenes were crushed and Soxhlet cleaned with heptane to decrease the concentration of coprecipitated/occluded compounds that were not extracted through the standard cleaning procedure.

C_7 asphaltenes were fractionated following the extrography method published in the second part of this series.[46] By this method, asphaltenes are selectively separated into fractions that ionize efficiently in APPI and later fractions that exhibit lower MIY. Briefly, asphaltenes were adsorbed on silica gel (5 mg of asphaltenes/1 g of SiO_2). The mixture asphaltene/SiO_2 was Soxhlet extracted with acetone, ACN, heptane, 1:1 Hep/Tol, Tol, 1:1 Tol/THF, THF, and 4:1 THF/MeOH. The fractionation was performed in triplicate for each asphaltene sample. The fractions were dried under N_2, weighed, and stored in the dark for subsequent FT-ICR MS analyses and precipitation tests.

Positive-Ion Atmospheric Pressure Photoionization Fourier Transform Ion Cyclotron Resonance Mass Spectrometry [(+) APPI FT-ICR MS]. Wyoming Deposit and Athabasca Bitumen C_7 asphaltenes and their extrography fractions were dissolved in toluene at a concentration of 200 μg/mL and directly infused into a Thermo-Fisher Ion Max APPI source (Thermo-Fisher Scientific, Inc., San Jose, CA). Mass spectrometry analyses were carried out with a custom-built 9.4 T Fourier transform ion cyclotron resonance mass spectrometer with data collection facilitated by a modular ICR data acquisition system (PREDATOR).[64,65] The conditions for MS and Tandem/MS analyses are reported in the first part of this series.[46] Data analysis and visualization were performed with PetroOrg N-16.0 Software.[66]

Precipitation Tests in Hep/Tol. Asphaltene samples and subfractions were dissolved in toluene and subsequently mixed with 20%, 40%, 60%, 80%, and 90% v/ v of heptane, under sonication for 1 h. The final asphaltene concentration was 1.1 wt % for all the precipitation tests. After 24 h, the mixtures were centrifuged at 5000 rpm to recover precipitated (unstable) asphaltenes. Precipitated materials and remnant solutions were dried under N_2 and weighed. Precipitation tests were performed in triplicate.

RESULTS AND DISCUSSION

Asphaltenes of Different Geological Origin Are Compositionally and Structurally Diverse. In the first manuscript of the series *Advances in Asphaltene Petroleomics*, it was hypothesized that the dominant asphaltene structure, island or archipelago, is sample dependent. We based this hypothesis on several reports on the composition of asphaltene products from mild pyrolysis and thermal cracking. Therefore, the work presented herein aims to scrutinize the compositional and structural differences between two asphaltene samples of different geological origin that produce very different pyrolysis product yields. For this purpose, we isolated C_7 asphaltenes from an organic deposit from a Wyoming oil well with known deposition issues due to natural depletion and high pyrolysis coke yield (island dominant).[54,62] Athabasca Bitumen, the largest reservoir of crude bitumen in the world,[67] was selected as the second asphaltene source, as its pyrolysis coke yield is 6-fold lower (archipelago dominant) than that of the Wyoming deposit.

As the two previous manuscripts in this series have highlighted selective ionization issues, care must be taken in the interpretation of direct APPI mass spectral results of unfractionated asphaltenes. However, given the large difference in coke yields and distillable pyrolysis products between the two samples, the broad-band, direct infusion results are compared in Figure 1. Figure 1 highlights the mass spectrometry results of whole C_7 asphaltene samples isolated from Wyoming Deposit (top) and Athabasca Bitumen (bottom), as described in the Experimental Section. It includes the broad-band molecular weight distributions (MWD), zoom-mass insets at m/z 450, and heteroatom group distributions derived from the elemental formulas assigned to all mass spectral peaks. Wyoming Deposit asphaltenes, with a MWD between $m/z \approx 250$ and 780, are enriched with polar heteroatomic groups O_xS_y and O_x, lack vanadyl porphyrins (group $N_4O_1V_1$), exhibit a high relative abundance of ions with low mass defect (0.10−0.20, indicative of highly aromatic, hydrogen-deficient species), and reveal a low mass spectral complexity (69 peaks in one nominal mass window at m/z 450). Conversely, Athabasca Bitumen asphaltenes are composed of a high relative abundance of peaks between $m/z \approx 475$ and 620, assigned as $N_4O_1V_1$ species. The sample is also enriched in S_x species, exhibits a greater spectral complexity (104 peaks at m/z 450), and is composed of ions that display a wide range of mass defects (between 0.05 and 0.45). Although the direct mass spectral analysis of unfractionated asphaltenes was previously shown to be biased toward species that have a low tendency to form nanoaggregates (island) and thus exhibit high ionization efficiency (monomer ion yield), these spectral features suggest that Athabasca Bitumen asphaltenes are a mixture of highly aromatic (hydrogen deficient, low mass defect) and alkyl-enriched species (hydrogen rich, high mass defect), consistent with a higher degree of structural diversity.[1,47,68]

To facilitate visualization of these compositional differences, assigned elemental compositions are grouped by their heteroatom content (e.g., species that contain a single sulfur atom in their elemental composition reside in the S_1 class) and displayed as a two-dimensional plot of double-bond equivalents (DBE, number of rings + double bonds) versus carbon number. Figure 2 presents the subsequent color-contoured isoabundance

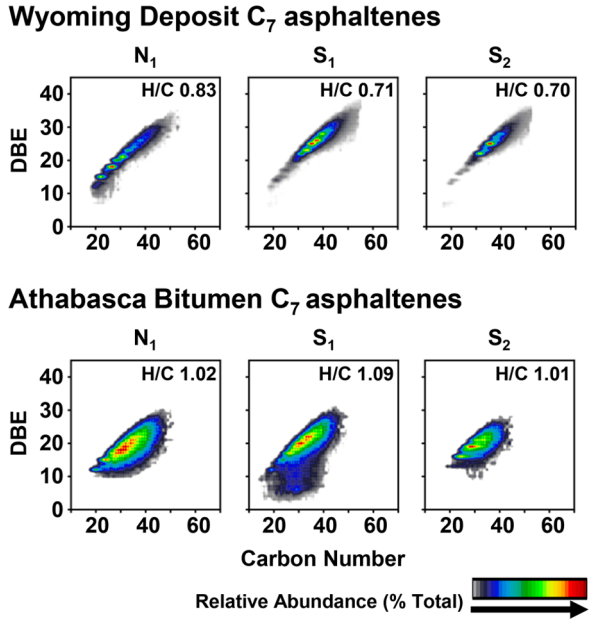

Figure 2. Color-contoured isoabundance plots of DBE versus carbon number for N_1, S_1, and S_2 heteroatom classes for (top) whole Wyoming Deposit C_7 asphaltenes and (bottom) whole Athabasca Bitumen C_7 asphaltenes.

DOI: 10.1021/acs.energyfuels.8b01765
Energy Fuels 2018, 32, 9106−9120

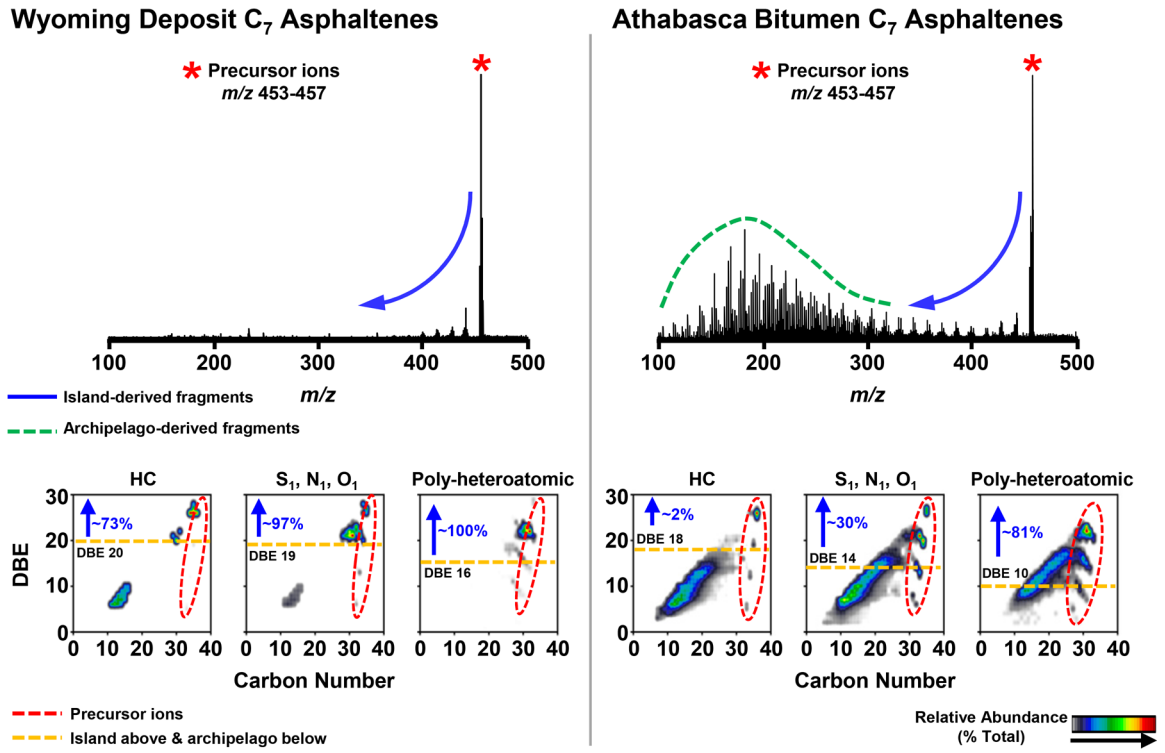

Figure 3. Fragmentation spectra and combined color-contoured isoabundance plots of DBE versus carbon number for hydrocarbons, monoheteroatomic, and polyheteroatomic classes for precursor and fragment ions derived from (left) Wyoming Deposit C_7 asphaltenes and (right) Athabasca Bitumen C_7 asphaltenes.

plots of DBE versus carbon number for the classes N_1, S_1, and S_2 for Wyoming Deposit (top) and Athabasca Bitumen (bottom) C_7 asphaltenes. Wyoming Deposit resembles the composition of "classical" asphaltenes,[48,69−71] as the compositional space of the classes S_1 and S_2 is shifted toward DBE values greater than 20 with a high relative abundance of compounds near the PAH limit (low mass defect) and short homologous series. These compositional features suggest that Wyoming Deposit asphaltenes are enriched with highly aromatic alkyl-deficient structures, further supported by the N_1 class, which exhibits discrete relative abundance maxima that lie on the PAH limit line at DBE values of 12, 15, and 18 (alkyl-deficient N-containing aromatic cores).

Athabasca Bitumen asphaltenes (Figure 2, bottom) are notably less aromatic (H/C > 1) than the Wyoming deposit asphaltenes. The compositional space, particularly that of the S_1 class, shows a predominate low-DBE region (as low as DBE ≈ 3). It exhibits a high concentration of species close to the PAH limit but contains longer homologous series (greater content of saturated moieties (CH_2 units)) compared to the Wyoming Deposit asphaltenes. Abundance-weighted H/C ratios, also presented in Figure 2, reveal that Wyoming deposit asphaltenes are composed of abundant hydrogen-deficient structures, whereas Athabasca Bitumen asphaltenes exhibit H/C ratios closer to the common bulk values (H/C ≈ 1.1) reported for petroleum asphaltenes.[72,73]

Fragmentation Behavior of Unfractionated Asphaltenes. Figure 3 reveals the striking difference in IRMPD fragmentation behaviors of whole Wyoming Deposit (left) and Athabasca Bitumen (right) C_7 asphaltenes. Precursor ions at m/z 453−457 were isolated with a mass-resolving quadrupole, transferred to the ICR cell, and subjected to infrared irradiation for 50−2000 ms. Under these conditions, model compounds undergo fragmentation of both saturated moieties (dealkylation) and archipelago bridges (i.e., alkyl and aryl linkages). However, aromatic cores remain intact during IRMPD.[46] Figure 3, top, shows the fragmentation spectra after 1000 ms of infrared irradiation. The composition of fragments and precursor ions is represented in the bottom of Figure 3 by combined plots of DBE versus carbon number for hydrocarbons (HC), monoheteroatomic species (S_1, N_1, and O_1), and polyheteroatomic compounds (e.g., S_2, N_1O_1, O_2, O_3). The yellow dotted line represents the island/archipelago boundary, calculated as the abundance weighted average DBE of the precursor ions minus the abundance weighted standard deviation.[47] The fragmentation spectrum of Wyoming Deposit asphaltenes reveals predominantly dealkylation (very low abundance of low m/z fragments), and is consistent with the fragments observed for PAH model compounds reported previously.[46] These results clearly suggest that the majority of compounds from the Wyoming Deposit asphaltenes are PAH's with few alkyl groups. The DBE versus carbon number plots for hydrocarbons and monoheteroatomic species demonstrate that most of the fragments (~73% and ~97%, respectively) have DBE values equal to/above the island/archipelago boundary (DBE = 20 and 19). Polyheteroatomic species also exhibit fragmentation that correlates with abundant island motifs: ~100% of the fragments have DBE values equal to/above the island/archipelago limit at DBE = 16. Thus, the fragmentation behavior of whole Wyoming Deposit asphaltenes clearly suggests that island structures are dominant.

The fragmentation pattern of Athabasca Bitumen asphaltenes (Figure 3, right) is dramatically different than that of the Wyoming deposit asphaltenes. The fragmentation spectrum is comprised of two well-defined pathways: dealkylation, (highlighted in Figure 3, top right with the blue arrow) where

DOI: 10.1021/acs.energyfuels.8b01765
Energy Fuels 2018, 32, 9106−9120

precursors lose carbon number but not aromaticity, in addition to a low molecular weight distribution between $m/z \approx 100$ and 300, composed of fragments with a lower carbon number and lower DBE than the precursor ions (highlighted with the green dotted line). The DBE versus carbon number plots suggest that Athabasca Bitumen asphaltenes are enriched with HC and monoheteroatomic archipelago motifs: ~98% and ~70% of the fragments exhibit DBE values below the island/archipelago boundary (DBE = 18 and 14, respectively). The polyheteroatomic fragments (of polyheteroatomic precursors) display a fragmentation pattern consistent with island-type structures: 81% of the fragments present DBE values equal to/above the island/archipelago boundary (DBE = 10). Such behavior is consistent with polyheteroatomic species in which all heteroatoms reside in a single, polyaromatic core. Simply, detection of polyheteroatomic species after fragmentation requires that all heteroatoms of a given class (e.g., $N_1O_1S_1$, S_3, N_1O_3) exist within the same aromatic core. However, it does not exclude the coexistence of polyheteroatomic archipelago structures. If heteroatoms are located in separate, alkyl-linked aromatic cores they fragment to produce monoheteroatomic and/or hydrocarbon species.[46] Regardless of the initial class, fragmentation of Athabasca Bitumen asphaltenes produces species that have a significantly lower DBE (aromaticity) than the precursor ions. Thus, they are composed of abundant archipelago structural motifs. However, it is likely that the archipelago structures accessed in this work differ from the ones early suggested by Strausz et al.[58,74] in three characteristics. First, both asphaltene samples exhibit a molecular weight distribution between $m/z \approx 250$ and 850, in agreement with initial predictions by Boduszynski et al.[75−77] and later TRFD reports by Mullins et al.[78,79] Second, the original archipelago model suggested structures with more than 10 aromatic cores because the structure was based on a high, but incorrect, asphaltene molecular weight. It is more likely that actual archipelago structures comprise up to 4 aromatic cores, as recently reported by atomic force microscopy.[22,23] Third, the nature of the "archipelago bridges" will remain, for now, unaddressed, as it is not currently possible to determine if the bridges between the individual aromatic cores are aryl−aryl, alkyl chains, or/and multiple naphthenic rings. To that end, a detailed characterization of aryl−aryl and alkyl- and cycloalkyl-substituted model compounds is currently underway in order to determine correlations between dissociation energetics and the nature of the archipelago bridges; this will be the subject of a future publication.

Comprehensive Asphaltene Characterization Assisted by Extrography Fractionation. Tandem MS analyses of whole samples suggest that island structures are dominant for Wyoming Deposit asphaltenes, whereas Athabasca Bitumen asphaltenes are composed of abundant island and archipelago motifs. However, it has been demonstrated that mass spectral characterization of unfractionated asphaltenes has a critical limitation that arises from their intrinsic heterogeneous aggregation.[15,47,50] Thus, an extrography method designed to separate asphaltenes on the basis of aggregation trends (and therefore ionization efficiency in APPI) is used to extend MS characterization. In this separation, the first solvent series (acetone and acetonitrile) selectively extracts species with high monomer ion yield (high ionization efficiency). The second series, composed of heptane, toluene, tetrahydrofuran, and methanol, separates remnant asphaltenes by polarity, which possess much lower monomer ion yields (low ionization efficiency). Figure 4 includes bar graphs that summarize the mass percentage (gray bars, left y axis) and the MIY (red bars, right y axis) for each fraction from Wyoming Deposit (top) and Athabasca Bitumen (bottom) C_7 asphaltenes. Figure 4 also presents the mass recovery of the fractionation. Monomer ion yield denotes a relative measure of the production of monomer (nonaggregated) ions from petroleum-derived samples. Monomer ion yield is a value inversely proportional to the accumulation period required to accumulate a target number of ions at a given sample concentration. Thus, samples that efficiently ionize, such as aromatic crude oil fractions, require shorter accumulation time to hit a target number of ions, which translates into a higher monomer ion yield. Supporting Information Tables S1 and S2 show gravimetric results, accumulation period, and MIY for whole samples and fractions. Wyoming Deposit asphaltenes are enriched in acetone (~35.1 wt %) and toluene (~31.8 wt %) fractions, whereas Athabasca Bitumen asphaltenes exhibit a high concentration of species that elute with Tol/THF (~41.5 wt %). Both samples exhibit a depleted mass in the ACN and THF fractions (<0.2 wt %). The greatest monomer ion yield is noted in the acetone fraction for both asphaltene samples, which decreases for the second solvent series as a function of increasing polarity. For example, the acetone fraction from Wyoming Deposit (MIY = 50.00) presents ~90-fold greater monomer ion yield than the toluene fraction (MIY = 0.55). Athabasca Bitumen asphaltenes have a similar trend; the acetone fraction exhibits ~30-fold greater monomer ion yield (MIY = 10.00) than the toluene fraction (MIY = 0.33). Importantly, the ~5× difference in MIY between the acetone fractions of each sample (Wyoming deposit ≈ 50 and Athabasca Bitumen ≈ 10) suggests that the acetone fractions from both asphaltenes are compositionally/structurally different.

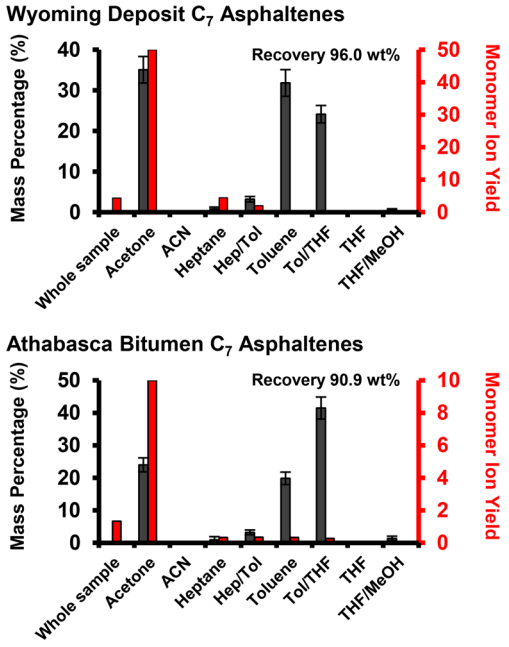

Figure 4. Mass recovery, mass distribution, and monomer ion yield for the extrography fractions derived from Wyoming Deposit (top) and Athabasca Bitumen (bottom) C_7 asphaltenes.

The mass recovery and the mass distribution of the fractions suggest that Athabasca Bitumen asphaltenes exhibit stronger

DOI: 10.1021/acs.energyfuels.8b01765
Energy Fuels 2018, 32, 9106−9120

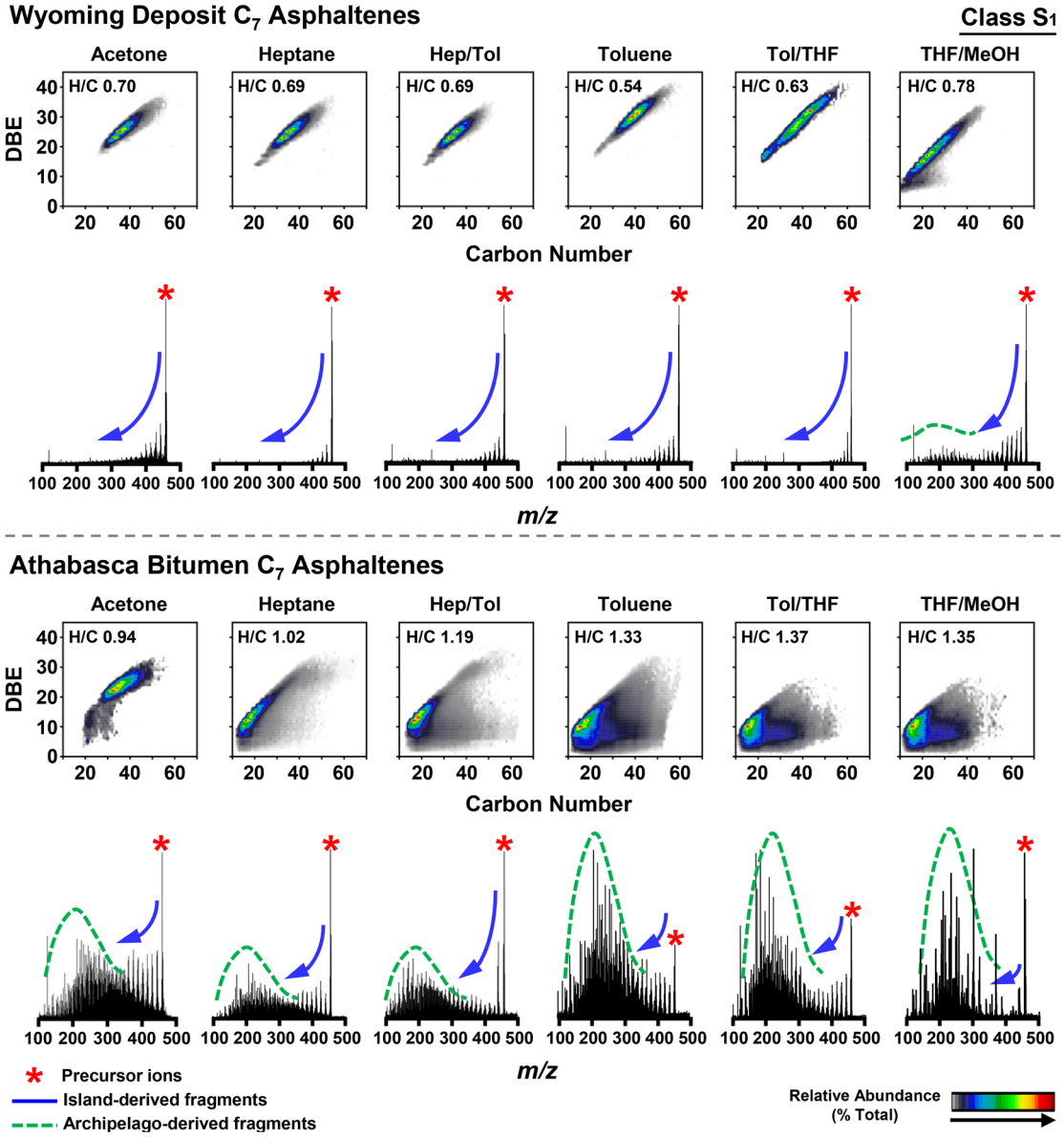

Figure 5. Color-contoured isoabundance plots of DBE versus carbon number for the class S_1 and fragmentation spectra of precursor ions at m/z 453−457 for the extrography fractions derived from Wyoming Deposit Asphaltenes (top panel) and Athabasca Bitumen (bottom panel) C_7 asphaltenes.

adsorption on the SiO_2 stationary phase. Although the mass recovery for Athabasca Bitumen is slightly lower (~90.9 wt %) than that for Wyoming Deposit asphaltenes (~96.0 wt %), more than ~42.0 wt % of the sample is extracted in the three latest/polar fractions (Tol/THF, THF, and THF/MeOH), whereas only ~25.0 wt % of Wyoming Deposit is recovered in the latest fractions.

Selective Isolation of Asphaltene Fractions with High Monomer Ion Yield Enables Observation of Otherwise Undetected Species. Figure 5 presents a compositional and structural comparison between Wyoming Deposit (top panel) and Athabasca Bitumen (lower panel) asphaltenes enabled by extrography fractionation coupled with APPI FT-ICR MS and IRMPD. Figure 5 includes plots of DBE versus carbon number for the class S_1 (without fragmentation) and fragmentation spectra derived from IRMPD of precursor ions at m/z 453−457. ACN and THF fractions are excluded due to their low concentration (<0.2 wt %) in the whole samples. Figures S1−S7 of the Supporting Information present DBE versus carbon number plots for the classes HC, N_1, O_1, S_2, S_3, $N_1O_1S_1$, and N_1S_1. All of the fractions derived from Wyoming Deposit exhibit a classical (island-type) asphaltene composition. In terms of DBE and carbon number, the acetone fraction resembles the composition of the unfractionated sample. Importantly, homologous series length decreases as a function of increasing fraction number. For instance, at DBE 30, acetone, Hep, Hep/Tol, Tol, Tol/THF, and THF/MeOH fractions, respectively exhibit 17, 16, 15, 12, 10, and 10 compositions. Additionally, from Hep to Tol/THF, the compositional space shifts toward higher DBE, which indicates increased adsorption of highly aromatic/alkyl-deficient compounds. Finally, the last fraction, extracted THF/MeOH, is enriched with species clustered close to PAH limit at lower carbon number and lower aromaticity. It is important to highlight that THF/MeOH is the only polar/protic mixture in both solvent series, capable of disrupting hydrogen bonding between asphaltene functionalities and silanol groups on SiO_2. These results agree with Boduszynski's continuum model, which predicts a lower carbon number and decreased

DOI: 10.1021/acs.energyfuels.8b01765
Energy Fuels 2018, 32, 9106−9120

aromaticity for highly polar petroleum species.[76,80−82] Abundance-weighted atomic ratios O/C, N/C, and S/C, provided in the Supporting Information Figure S8, demonstrate that the latest fractions are enriched with O-containing functionalities, which suggests that oxygen content plays a critical role in asphaltene adsorption on SiO_2.[83]

The acetone fraction from Athabasca Bitumen presents a classical asphaltene composition with abundant compounds with DBE values above 20 and a well-defined planar limit. However, even in the Bitumen acetone fraction we see a small relative abundance of surprisingly low DBE compounds (DBE < 18). The remaining fractions exhibit a high relative abundance of species with atypically low DBE values and long homologous series. For instance, the heptane fraction is composed of abundant compounds clustered at the PAH limit, with DBE values as low as 7 and carbon number ranging between ∼12 and 50. As the polarity of the second solvent series increases, the compositional space is enriched with more saturated species (higher content of CH_2 units). Tol/THF and THF/MeOH fractions exhibit abundant compounds with DBE values between 7 and 15 and carbon number greater than 40. The classical view of asphaltene structure dictates that most of the unsaturation (DBE) is part of a single-fused aromatic core.[13] Given this case, abundant S_1 species detected in the latest fractions, with DBE = 7 and DBE = 10, could be benzothiophene (2-ring) and dibenzothiophene (3-ring) cores having one fused cycloalkane ring and ∼15−25 CH_2 units in alkyl side chains. These structures are not consistent with strong adsorption on SiO_2 or the classical nanoaggregation mechanism for petroleum asphaltenes, where large fused aromatic cores undergo π stacking to produce stable aggregates.[13,18] Indeed, these elemental compositions are also abundant in aromatic/resin fractions from heavy oils, which exhibit high solubility in heptane and efficient ionization in APPI.[48,80,84−86] Thus, it is important to reiterate that all extrography fractions derived from Wyoming Deposit and Athabasca Bitumen fit into the solubility definition of asphaltenes: the fractions are heptane insoluble and toluene soluble. In effect, the solubility in toluene decreases as a function of increasing fraction number (discussed below).[47] Thus, the reason for the strong adsorption on SiO_2 and the decreased solubility of these fractions in Hep/Tol appears puzzling.

Separation of asphaltenic samples into fractions with distinctive MIY exposes extensive compositional differences between Wyoming Deposit and Athabasca Bitumen asphaltenes. Infrared multiphoton dissociation demonstrates that all fractions from Wyoming Deposit (Figure 5, upper panel) preferentially exhibit dealkylation fragmentation. Moreover, under optimized IRMPD conditions,[46] precursors are the most abundant ions in the broad-band fragmentation spectra. This behavior strongly suggests that island is the dominant structure in Wyoming Deposit asphaltenes. On the other hand, the fragmentation behavior of Athabasca Bitumen fractions suggests abundant archipelago motifs. All of the extrography fractions exhibit the island-distinctive dealkylation fragmentation at high m/z and the low-molecular weight distribution that arise from the dissociation of archipelago structures composed of small PAHs.[16,46] The acetone fraction exhibits comparable abundance of the dealkylation pattern and the low MWD, suggesting similar amounts of island and archipelago motifs. As the polarity increases during the second solvent series, the abundance of the precursors (relative to the fragment ions) decreases; the distribution of fragments is enriched in the low MWD. The latest fractions, Tol/THF and THF/MeOH, are depleted in highly aromatic island-type compounds and exhibit the highest relative abundance of fragments consisting of small PAHs (with $m/z \approx 100-300$, discussed below). It is worth highlighting that the higher concentration of archipelago structures in Athabasca Bitumen acetone fraction may be the reason behind the 5-fold lower monomer ion yield when compared with the island-dominant acetone fraction derived from Wyoming Deposit asphaltenes.

Need for a New Molecular Definition of Asphaltenes. The insolubility of asphaltenes in paraffinic solvents has been attributed to their highly aromatic/alkyl-deficient nature that promotes strong aggregation by π stacking, which is known as the Yen-Mullins model.[13,18] On this basis, the compositional space of petroleum asphaltenes should be enriched with pericondensed compounds clustered at the PAH limit, with DBE values greater than ∼20 (more than ∼7 fused rings) and depleted content of CH_2 units (short homologous series/less steric hindrance). However, the composition of more than ∼60 wt % of Athabasca Bitumen asphaltenes does not match the classical asphaltene model. Figure 6 presents plots of DBE versus carbon number for the classes S_1, S_2, S_3, O_1S_1, O_1S_2, and O_2S_1 for the toluene fraction extracted from Athabasca Bitumen C_7 asphaltenes.

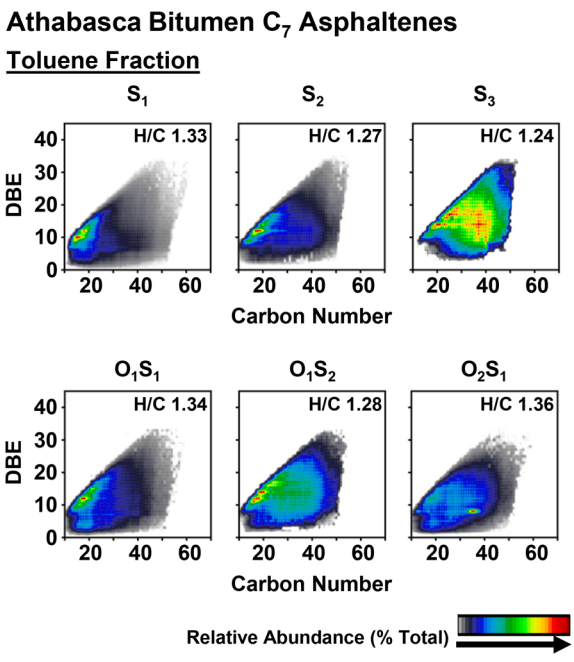

Figure 6. Color-contoured isoabundance plots of DBE versus carbon number for the classes S_1, S_2, S_3, O_1S_1, O_1S_2, and O_2S_1 for the toluene fraction extracted from Athabasca Bitumen C_7 asphaltenes.

carbon number for S-containing classes such as S_1, S_2, S_3, O_1S_1, O_1S_2, and O_2S_1 for the toluene fraction extracted from Athabasca Bitumen asphaltenes. The compositional space of the class S_3, composed of a high relative abundance of species with carbon number as high as ∼50 and low DBE values between 6 and 12, is highly atypical. In fact, the lower DBE limits for the S_1, S_2, and S_3 classes are 1, 2, and 3 DBE and thus must contain sulfidic functionalities. Similarly, Rogel, and Schuler et al. also reported atypical compositions for asphaltene samples from diverse geological origin. These findings suggest the need for a new molecular description of petroleum asphaltenes.[22,87,88]

It is important to highlight that all extrography fractions fit into the solubility definition of petroleum asphaltenes. Figure 7 illustrates the precipitation trends when whole asphaltene

DOI: 10.1021/acs.energyfuels.8b01765
Energy Fuels 2018, 32, 9106−9120

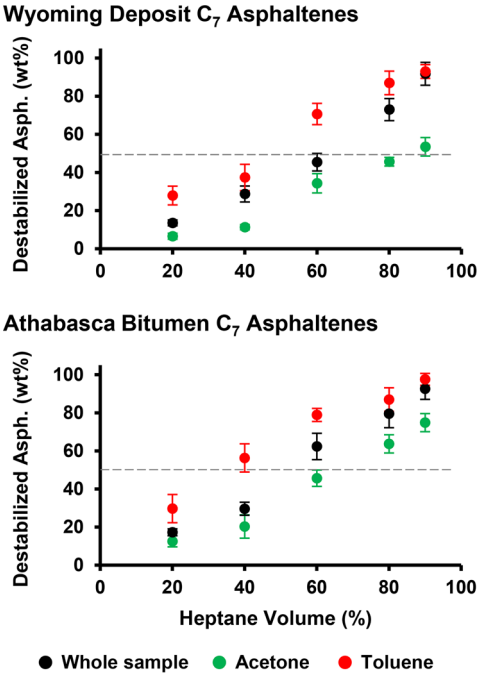

Figure 7. Precipitation mass percentage versus titrated volume percentage of heptane in toluene solution for whole samples, acetone, and toluene fractions derived from Wyoming Deposit (Top) and Athabasca Bitumen (bottom) C_7 asphaltenes.

samples and fractions (acetone and toluene) are titrated with heptane. For whole Wyoming Deposit asphaltenes, the addition of 20% v/v of heptane induces the precipitation of ~14 wt % of the sample, whereas titration with 60% and 90% v/v of heptane results in the precipitation of ~45 and ~92 wt % of the sample. On the other hand, the acetone fraction, with the highest monomer ion yield, exhibits increased stability in Hep/Tol. With 20% v/v of heptane, only ~7 wt % is precipitated, whereas the addition of 90% v/v of heptane only precipitates ~54 wt % of the fraction. Conversely, the toluene fraction is less stable. The addition of 20% and 90% v/v of heptane promotes the precipitation of ~28 and ~93 wt % of the fraction. Combined with structural and compositional information given in Figure 5, precipitation results demonstrate that Wyoming Deposit asphaltenes agree with the Yen-Mullins model: the aggregation/precipitation is stronger for fractions with higher DBE and fewer alkyl side chains (less steric hindrance).[13,19,89]

Athabasca Bitumen asphaltenes exhibit similar precipitation trends. However, the acetone fraction appears to be less stable than that from the Wyoming Deposit; the addition of 90% v/v of heptane causes precipitation of ~75 wt % of the fraction. Importantly, ~98 wt % of the toluene fraction is precipitated by addition of 90% v/v of heptane. Therefore, regardless of the atypical composition (low DBE/high carbon number), the toluene fraction from Athabasca Bitumen matches the solubility definition of asphaltenes. All of the extrography fractions extracted after acetone are *insoluble* in heptane and *soluble* in toluene. Moreover, the precipitation data at 90% v/v suggest that the solubility in toluene decreases as a function of increasing fraction number. Indeed, toluene, Tol/THF, and THF/MeOH fractions require heating/sonication for solubilization in toluene. These results agree with the solubility behavior of asphaltene fractions previously reported by Gawrys,[49] Speckter,[50] and Kaminski et al.,[90] who reported an inverse correlation between fraction polarity and asphaltene solubility in toluene. It is worth highlighting that given that the compositional space of the latest fractions from Athabasca Bitumen differ from the classical definition of asphaltenes, the reason for their solubility

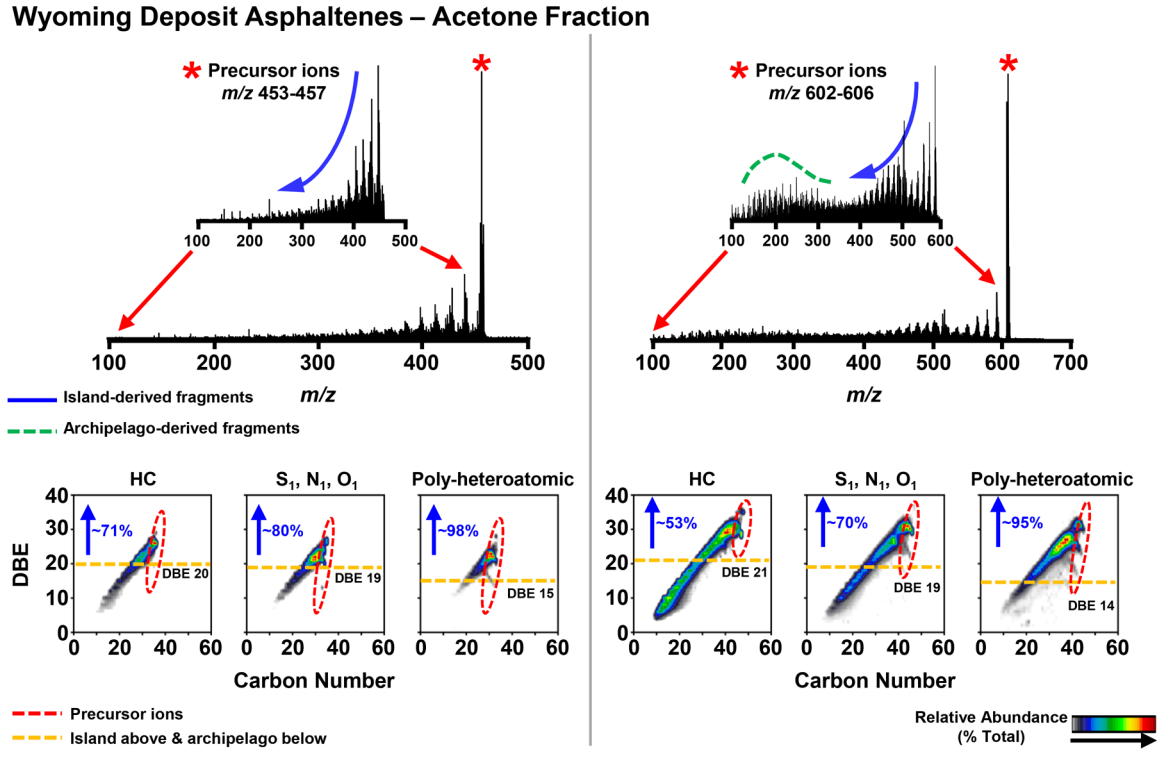

Figure 8. Fragmentation spectra and combined color-contoured isoabundance plots of DBE versus carbon number for precursor and fragment ions for m/z (left) 453−457 and (right) m/z 602−606 for the acetone fraction from Wyoming Deposit C_7 asphaltenes.

DOI: 10.1021/acs.energyfuels.8b01765
Energy Fuels 2018, 32, 9106−9120

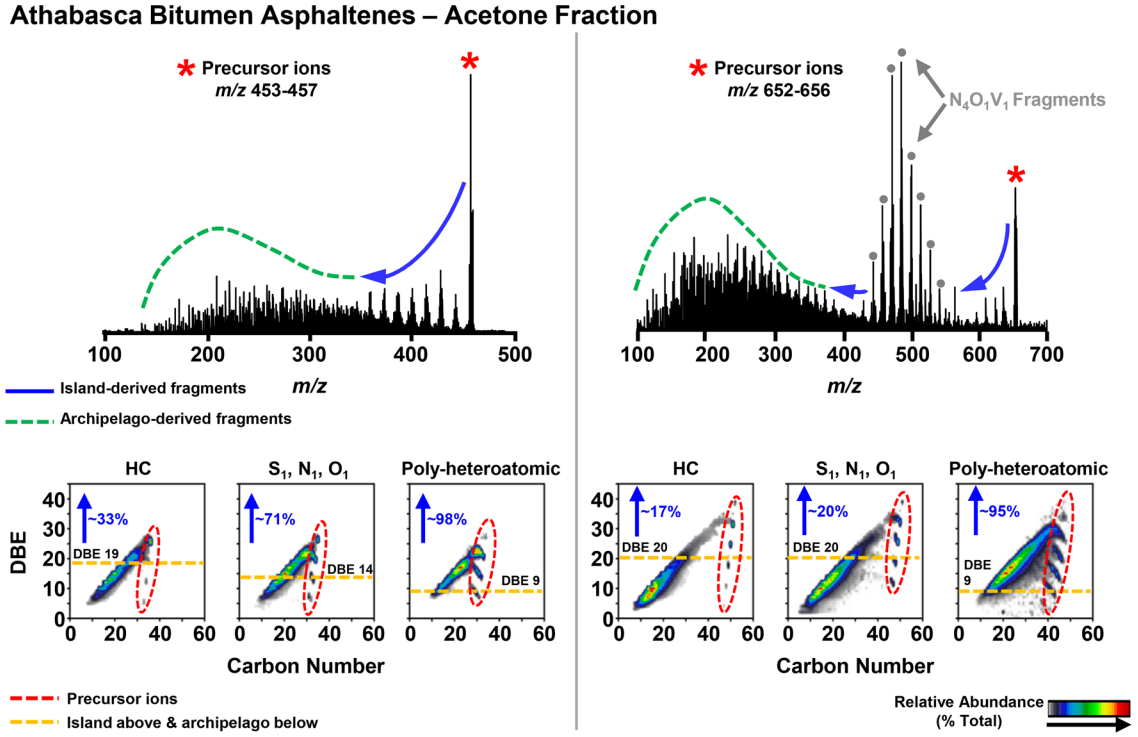

Figure 9. Fragmentation spectra and combined color-contoured isoabundance plots of DBE versus carbon number for HC, monoheteroatomic, and polyheteroatomic precursor and fragment ions for m/z (left) 453−457 and (right) m/z 652−656 for the acetone fraction from Athabasca Bitumen C_7 asphaltenes.

behavior should be explained by a model different than the Yen-Mullins theory.

Importance of Stucture and Functionality. It is apparent from the data in Figures 5 and 6 that both structure and chemical functionality are driving factors in the elution of compounds from the silica gel surface. For example, we observe a clear shift in the DBE distributions of the S_1 class for Athabasca Bitumen asphaltenes with elution order. The toluene fraction shows a high relative abundance of low DBE ions ranging down to DBE values of 1. This indicates the clear presence of sulfides and/or thiols in these fractions. However, this atypical composition is not the case for all samples, yet sulfur classes are still present in later eluting fractions. It was shown in the second paper of this series that compounds of the same molecular formula elute in drastically different solvent compositions (e.g., acetone and Tol:THF) and, further, that those compositions revealed different types of fragmentation pathways (i.e., compositions in the acetone fractions showed island-type dealkylation, and compositions in the Tol−THF fraction showed more archipelago-type fragmentation with dealkylation and loss of aromaticity). This trend was highlighted with high-DBE ions from the S_1 class. This is of special interest, as these sulfur compounds are likely thiophenic in nature. As such, the observed S-compounds are nonpolar and should not exhibit such varied elution behavior. However, the fact that compounds elute under such drastically different solvent compositions and show different fragmentation pathways suggests that structure also plays a role in the retention of the silica surface. Gray, Sjöblom, and Kilpatrick et al.[91−93] have all previously pointed out the analogy between asphaltenes and proteins. Gray and co-workers demonstrated that adsorption of asphaltene samples on kaolinite is kinetically limited (like proteins) and proposed that conformational changes of asphaltenes could increase surface contact, which may induce low rates of desorption.[91] Along similar lines, Spiecker, Sauerer, and Kilpatrick et al.[93−95] demontrated long equilibration periods for asphaltenes and their polar fractions adsorbing at oil/water interfaces; this behavior could be ascribed to asphaltene slow diffusion and slow rearrangement. This phenomenon, by which archipelago structural motifs possess the conformation freedom necessary to maximize surface interactions, may explain the difference in retention for nonpolar isomeric species present in asphaltenes. It may also explain the decrease in solubility associated with later-eluting fractions. Whatever the reason, it is obvious that the retention of asphaltenes on silica gel is complex and merits further investigation.

Asphaltene Samples, Always a Mixture of Island and Archipelago? Figure 8 presents the fragmentation spectra of isolated ions at m/z 453−457 (left) and m/z 602−606 (right) for the sample with the highest contribution of island motifs: the acetone fraction extracted from Wyoming Deposit asphaltenes. The zoom-mass insets exclude the precursor ions and facilitate visualization of island and archipelago fragments. Fragment ions derived from precursors at m/z 453−457 exhibit a dominant contribution of island structures; the dealkylation "decay pattern" is the prevailing fragmentation route, and the low MWD presents a decreased abundance. However, an increase of ~150 Da in the mass isolated segment (to $602 < m/z < 606$) reveals a greater content of archipelago motifs; the zoom mass inset (Figure 8, right) demonstrates that in addition to the abundant dealkylation fragmentation between $m/z \approx 300$ and 600 there is a low molecular weight distribution between $m/z \approx$ 100 and 300. The DBE versus carbon number plots indicate that HC, monoheteroatomic, and polyheteroatomic species with m/z 453−457 are enriched with island structures: the majority of the fragments (~71%, ~80%, and ~98%, respectively) exhibit

DOI: 10.1021/acs.energyfuels.8b01765
Energy Fuels 2018, 32, 9106−9120

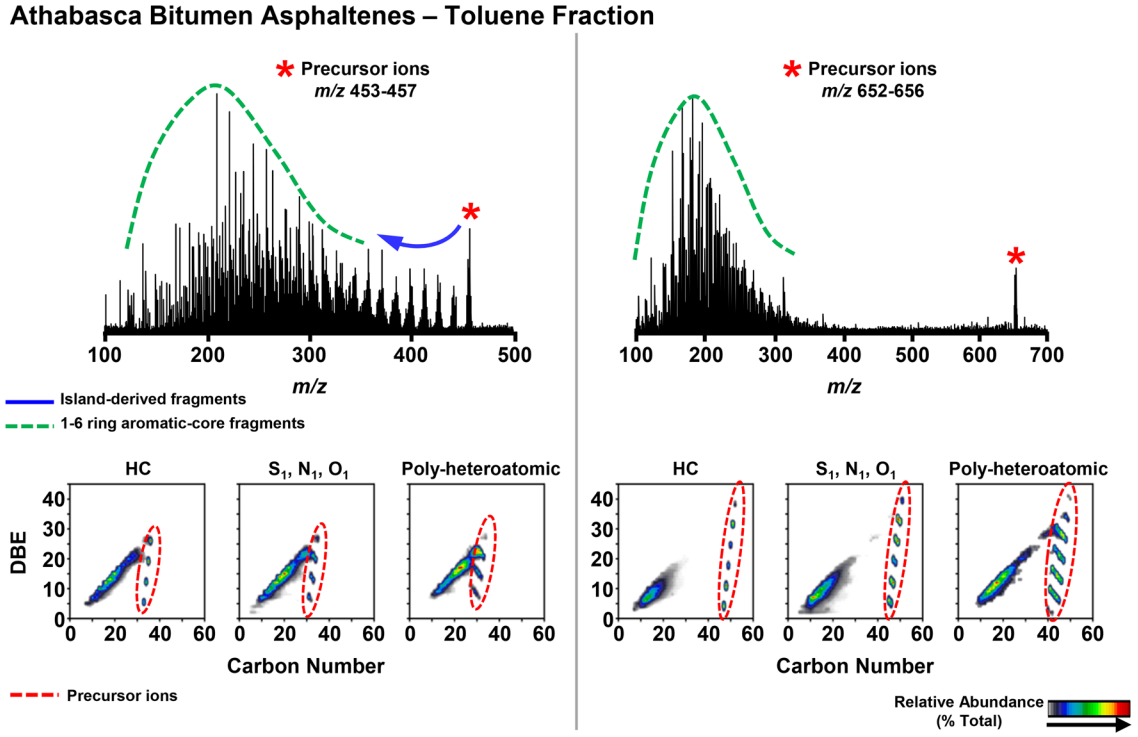

Figure 10. Fragmentation spectra and combined color-contoured isoabundance plots of DBE versus carbon number for HC, monoheteroatomic, and polyheteroatomic precursor and fragment ions for m/z (left) 453−457 and (right) m/z 652−656 for the toluene fraction from Athabasca Bitumen C_7 asphaltenes.

DBE values equal to/above the island/archipelago boundary. On the other hand, fragmentation of precursor ions at m/z 602−606 reveals abundant hydrocarbons (~47%) and monoheteroatomic fragments (~30%) derived from archipelago motifs and evidence for the existence of polyheteroatomic archipelago structures, as indicated by the detection ~5% of polyheteroatomic fragments with DBE values between 5 and 13, below the island/archipelago boundary. These results suggest that even island-dominant samples exhibit, to some extent, a contribution of archipelago structures.

Closer Inspection of Bitumen Asphaltene Fragmentation. The composition and structure of the bitumen asphaltenes (and associated extrography fractions) offer a unique opportunity to evaluate the ability of APPI FT-ICR MS with IRMPD to detect and characterize island and archipelago structural motifs. Specifically, the high relative abundance of vanadyl porphyrins ($N_4O_1V_1$ class), which are a known structural class and known to be island in nature, provides a unique molecular class and known structural motif to evaluate the IRMPD method. Figure 9 presents the IRMPD results from two different mass isolated windows, m/z 453−457 (left) and m/z 652−656 (right), along with their associated fragment plots of DBE versus carbon number for the bitumen asphaltene acetone fraction. The mass-isolated segment m/z 453−457 contains no porphyrin species, and as previously discussed, the IRMPD results demonstrate the characteristic island and archipelago fragmentation patterns. The higher mass-isolated segment (m/z 652−656) was specifically isolated because it was previously determined to contain alkylated vanadyl porphyrins.[96] As expected, the IRMPD results reveal abundant island, vanadyl porphyrin fragments as well as the lower MWD characteristic of archipelago species. Thus, the proposed methodology yields structural data that is consistent with known structural motifs in petroleum. In the current example, the determination of island versus archipelago motifs for the polyheteroatomic ions is difficult due to the wide distribution of DBE values present in the precursor ions. Thus, the ability to distinguish between high and low DBE precursor will be the discussion of a future manuscript.

The bitumen extrography toluene fraction offers another unique opportunity, as it contains a high relative abundance of "atypical" asphaltenes with low DBE values and wide carbon number ranges (Figure 5, bottom). Figure 10 presents the IRMPD results from 2 different mass isolated windows, m/z 453−457 (left) and m/z 652−656 (right), along with their associated fragment plots of DBE versus carbon number. As highlighted in the red ovals for both mass isolated segments, the "atypical" compositional space of this fraction results in the isolation of precursor ions that span an abnormally wide DBE range. In the lower mass isolated segment (m/z 453−457), distinct island and archipelago fragmentation patterns are clearly evident. However, the higher mass isolated segment (m/z 652−656) displays an overwhelming contribution of archipelago-type fragmentation. Despite the large contribution of the archipelago fragmentation pattern, special care must be taken in interpretation due to the wide DBE range of the precursor ions. Importantly, HC and monoheteroatomic precursor ions, with DBE values from 25 to 42, appear to be enriched with bridged PAHs (archipelago motifs): there is no production of HC, S_1, N_1, and O_1 fragments that span this high DBE range. The results clearly reveal abundant archipelago species; however, the high abundance of low DBE precursor ions also suggests abundant (highly alkylated small PAHs) island structures as well.

Planar Limit Slopes Predict a Higher Concentration of Archipelago Motifs at High *m/z*. DBE versus carbon number plots reveal additional structural information through the

DOI: 10.1021/acs.energyfuels.8b01765
Energy Fuels 2018, 32, 9106−9120

analysis of the planar limit slopes. Planar limits are the lines generated by connecting maximum DBE values at given carbon numbers.[97] Several reports suggest the use of planar limit slopes for understanding the molecular structure of petroleum.[70,97−99] For instance, Marshall et al.[100,101] demonstrated that the maximum value for the slope, for the compositional space of petroleum-derived samples, is ∼0.90 (known as the "90% rule"). Therefore, the maximum DBE value for a planar fossil hydrocarbon cannot exceed ∼90% of its carbon content. In another report, Cho et al.[84] suggested correlations between the slope and the structure of SARA fractions from crude oils. The authors concluded that the planar limit slope is ∼0.25 for saturated hydrocarbons, ∼0.75 for aromatics, and ∼0.90 for samples enriched with pericondensed PAHs (resins and asphaltenes).

The detailed inspection of the DBE versus carbon number plots given in Figure 5 reveals an interesting feature: the planar limit slope decreases as a function of increasing carbon number. Moreover, some classes exhibit a compositional space with two regions clearly defined by a different planar limit slope. Figure 11 highlights the change of the slope as a function of increasing carbon number for the class $S_2^{\bullet+}$ in the acetone and toluene fractions for Wyoming Deposit asphaltenes. Supporting Information Figures S9 and S10 include a detailed description about the calculation of the planar limit slopes. For an illustrative purpose, Figure 11 also shows examples of the variation of slope when the organization of aromatic rings follows different growth patterns.[97,100,102] The addition of carbon and hydrogen atoms to produce pericondensed structures generates planar limit slopes close to ∼0.90. When the addition of aromatic rings produces catacondensed compounds, the slope decreases to ∼0.75. On the other hand, on the addition of aromatic rings to generate archipelago structures, where the bridges between the individual cores are either aryl−aryl or naphthenic rings, the slope decreases to ∼0.62. Blanco-Combariza et al.[102] reported an approach to extract structural information from FT-ICR MS data of fossil fuels on the basis of periodic tables of benzenoid hydrocarbons.[103−105] The authors suggested that compositions close to the PAH limit, with slopes near ∼0.90, are less diverse (fewer isomers) because they consist of pure pericondensed structures. As the molecular formulas move toward the right side of the homologous series or the planar limit slope decreases there is greater structural diversity: the benzenoid periodic tables predict the presence of catacondensed compounds and species with multiple cores linked by aryl−aryl bridges, like the archipelago structures found by Schuler et al.[23]

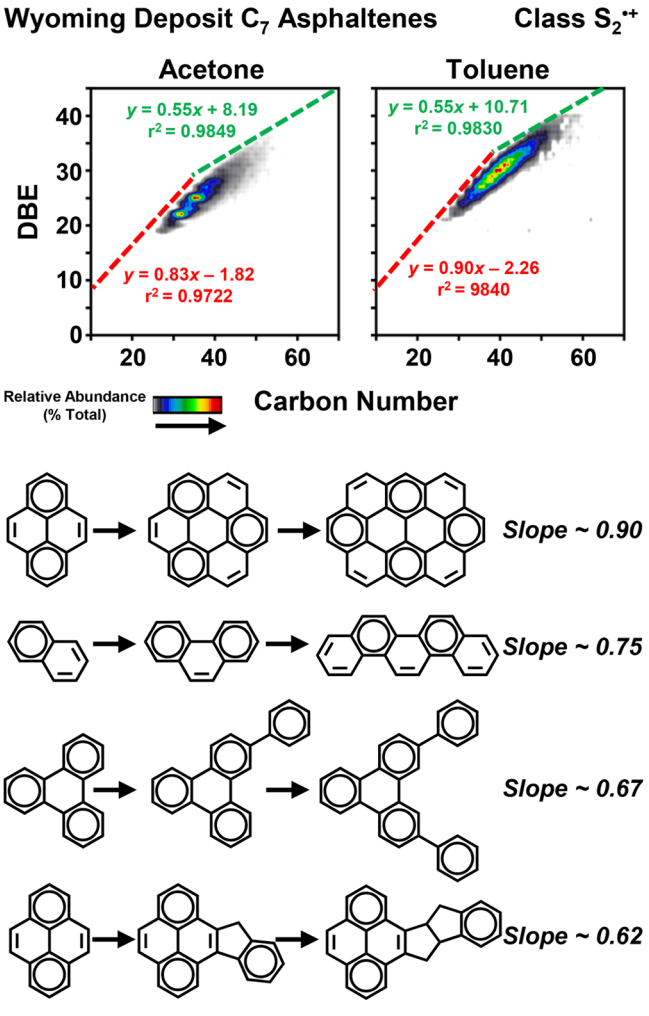

Figure 11. Color-contoured isoabundance plots of DBE versus carbon number for the class $S_2^{\bullet+}$ for the acetone and toluene fractions from Wyoming Deposit C_7 asphaltenes. Planar limits are highlighted with red and green dotted lines; plots include the planar limit equations. Effect of aromatic condensation and island/archipelago motifs on the slope is represented with model structures.

Figure 11 shows that low-DBE $S_2^{\bullet+}$ compounds (DBE < 30), contained in acetone and toluene fractions from Wyoming Deposit asphaltenes, exhibit planar limit slopes of 0.83 and 0.90. The turning point occurs between carbon numbers ∼35 and 38, where both slopes decrease to 0.55. This behavior suggests the existence of a "carbon limit" where the structure cannot support a higher pericondensation, and further addition of carbon and hydrogen atoms would likely produce catacondensed moieties or archipelago structures. In other words, the slope decreases as a function of increasing carbon number, which suggest that high-molecular weight asphaltenes exhibit a greater structural diversity through an increase in catacondensed structures and archipelago motifs. Supporting Information Figure S11 includes examples for the decrease of the planar limit slope as a function of increasing carbon number for additional samples: Athabasca Bitumen, Petrophase 2017, and South American Medium asphaltenes.

CONCLUSIONS

The direct infusion APPI FT-ICR MS analysis of two asphaltene samples that were previously shown to be island dominant (Wyoming Deposit) and archipelago dominant (Athabasca Bitumen) revealed that the Wyoming Deposit asphaltene sample had a lower spectral complexity with species that spanned a narrow distribution at low mass defect (hydrogen deficient). The bitumen asphaltene sample was more compositionally complex and contained species over a wider mass defect range (higher degree of alkylation). The fragmentation (IRMPD) of mass-isolated segments from each sample yielded fragmentation patterns consistent with their previously determined structure. The Wyoming Deposit asphaltene demonstrated island-dominated fragmentation patterns that slightly increased in archipelago-type fragments with increased molecular weight. The Athabasca bitumen asphaltene yielded abundant island and archipelago fragments that became increasing archipelago with increased mass. Both samples were subjected to an extrography fractionation method that isolated species of similar ionization efficiency, which facilitated

DOI: 10.1021/acs.energyfuels.8b01765
Energy Fuels 2018, 32, 9106−9120

detection of species with low monomer ion yield. The subsequent IRMPD analysis of these fractions confirmed the island dominance of the Wyoming Deposit asphaltene structure, as abundant archipelago fragments were only detected in the latest eluting fractions. The bitumen asphaltene was shown to contain abundant archipelago species in all extrography fractions, with "atypical" sulfur-containing asphaltenes that started to elute in the toluene fraction, and continued to the last extrography fraction. These atypical species were shown to contain sulfidic/thiol compounds, abundant archipelago structures, as well as highly alkylated island species. Finally, as previously documented in the literature, planar limit slopes were shown to correlate to structural type: island at slopes ∼0.9 (carbon numbers less than 35) and archipelago ∼0.5 (carbon numbers greater than 35). Thus, collectively these results provide strong evidence that both island and archipelago structural motifs are abundant in petroleum asphaltenes, and the ratio of each is sample dependent.

■ ASSOCIATED CONTENT

Supporting Information

The Supporting Information is available free of charge on the ACS Publications website at DOI: 10.1021/acs.energyfuels.8b01765.

DBE versus carbon number plots for the class HC for asphaltene extrography fractions (PDF)

DBE versus carbon number plots for the class N_1 for asphaltene extrography fractions (PDF)

DBE versus carbon number plots for the class O_1 for asphaltene extrography fractions (PDF)

DBE versus carbon number plots for the class S_2 for asphaltene extrography fractions (PDF)

DBE versus carbon number plots for the class S_3 for asphaltene extrography fractions (PDF)

DBE versus carbon number plots for the class $N_1O_1S_1$ for asphaltene extrography fractions (PDF)

DBE versus carbon number plots for the class N_1S_1 for asphaltene extrography fractions (PDF)

Abundance-weighted O/C, N/C, and S/C ratios for whole samples and extrography fractions (PDF)

Calculation of planar limit slopes for $S_2^{\bullet+}$ species the for acetone fraction from Wyoming Deposit asphaltenes (PDF)

Calculation of planar limit slopes for $S_2^{\bullet+}$ species for the toluene fraction from Wyoming Deposit asphaltenes (PDF)

Decrease of the planar limit slope as a function of increasing carbon number for Athabasca Bitumen, Petrophase 2017, and South American Medium asphaltenes (PDF)

Mass distribution and recovery percentage for Wyoming Deposit and Athabasca Bitumen Asphaltenes, monomer ion yield calculation for whole asphaltenes and fractions, and figure captions for Figures S1−S11 (PDF)

■ AUTHOR INFORMATION

Corresponding Author

*E-mail: rodgers@magnet.fsu.edu.

ORCID

Ryan P. Rodgers: 0000-0003-1302-2850

Notes

The authors declare no competing financial interest.

■ ACKNOWLEDGMENTS

This work was supported by the National Science Foundation (NSF) Division of Materials Research (DMR-1157490 and DMR-1644779), the Florida State University, the Florida State University Future Fuels Institute, and the State of Florida. The authors thank Don F. Smith, Chad Weisbrod, and Greg Blakney for help with data calibration and instrument performance and Yuri E. Corilo for PetroOrg software. The authors also thank Logan C. Krajewski for help with laser alignment for IRMPD experiments. The authors give a special thanks to Andrew Yen for providing Wyoming Deposit and Parviz Rahimi for providing Athabasca Bitumen.

■ REFERENCES

(1) Rodgers, R. P.; Marshall, A. G. *Asphaltenes, Heavy Oils and Petroleomics*; Springer: New York, 2007; pp 63−93.

(2) Hammami, A.; Ratulowski, J. *Asphaltenes, Heavy Oils, and Petroleomics*; Springer: New York, 2007; pp 617−660.

(3) Carbognani, L.; Espidel, J.; Izquierdo, A. *Asphaltenes and Asphalts, 2. Developments in Petroleum Science*; Elsevier B.V.: Amsterdam, The Netherlands, 2000; Vol. *40*, pp 335−362.

(4) Qiao, P.; Harbottle, D.; Tchoukov, P.; Masliyah, J.; Sjöblom, J.; Liu, Q.; Xu, Z. *Energy Fuels* **2017**, *31* (4), 3330−3337.

(5) Yarranton, H. W.; Hussein, H.; Masliyah, J. H. *J. Colloid Interface Sci.* **2000**, *228* (1), 52−63.

(6) Martínez-Palou, R.; Mosqueira, M. D. L.; Zapata-Rendón, B.; Mar-Juárez, E.; Bernal-Huicochea, C.; de la Cruz Clavel-López, J.; Aburto, J. *J. Pet. Sci. Eng.* **2011**, *75* (3−4), 274−282.

(7) Buckley, J. S. *Energy Fuels* **2012**, *26* (7), 4086−4090.

(8) Moulijn, J. A.; van Diepen, A. E.; Kapteijn, F. *Appl. Catal., A* **2001**, *212* (1−2), 3−16.

(9) Akbarzadeh, K.; Zhang, D.; Creek, J.; Jamaluddin, A. J.; Marshall, A. G.; Rodgers, R. P.; Mullins, O. C. *Oilfield Rev.* **2007**, *19* (2), 22−43.

(10) Tojima, M.; Suhara, S.; Imamura, M.; Furuta, A. *Catal. Today* **1998**, *43* (3−4), 347−351.

(11) Betancourt, S. S.; Ventura, G. T.; Pomerantz, A. E.; Viloria, O.; Dubost, F. X.; Zuo, J.; Monson, G.; Bustamante, D.; Purcell, J. M.; Nelson, R. K.; Rodgers, R. P.; Reddy, C. M.; Marshall, A. G.; Mullins, O. C. *Energy Fuels* **2009**, *23*, 1178−1188.

(12) Strausz, O. P.; Mojelsky, T. W.; Lown, E. M. *Fuel* **1992**, *71* (12), 1355−1363.

(13) Mullins, O. C. *Energy Fuels* **2010**, *24* (4), 2179−2207.

(14) Mullins, O. C. *Energy Fuels* **2009**, *23* (5), 2845−2854.

(15) Gray, M.; Tykwinski, R.; Stryker, J.; Tan, X. *Energy Fuels* **2011**, *25*, 3125−3134.

(16) Podgorski, D. C.; Corilo, Y. E.; Nyadong, L.; Lobodin, V. V.; Bythell, B. J.; Robbins, W. K.; McKenna, A. M.; Marshall, A. G.; Rodgers, R. P. *Energy Fuels* **2013**, *27* (3), 1268−1276.

(17) Rüger, C. P.; Neumann, A.; Sklorz, M.; Schwemer, T.; Zimmermann, R. *Energy Fuels* **2017**, *31*, 13144−13158.

(18) Mullins, O. C.; Sabbah, H.; Eyssautier, J.; Pomerantz, A. E.; Barré, L.; Andrews, A. B.; Ruiz-Morales, Y.; Mostowfi, F.; McFarlane, R.; Goual, L.; Lepkowicz, R.; Cooper, T.; Orbulescu, J.; Leblanc, R. M.; Edwards, J.; Zare, R. N. *Energy Fuels* **2012**, *26*, 3986−4003.

(19) Mullins, O. C. *Annu. Rev. Anal. Chem.* **2011**, *4*, 393−418.

(20) Tanaka, R.; Sato, E.; Hunt, J. E.; Winans, R. E.; Sato, S.; Takanohashi, T. *Energy Fuels* **2004**, *18* (7), 1118−1125.

(21) Yen, T. F.; Erdman, J. G.; Pollack, S. S. *Anal. Chem.* **1961**, *33* (11), 1587−1594.

(22) Schuler, B.; Fatayer, S.; Meyer, G.; Rogel, E.; Moir, M.; Zhang, Y.; Harper, M. R.; Pomerantz, A. E.; Bake, K. D.; Witt, M.; Pena, D.; Kushnerick, J. D.; Mullins, O. C.; Ovalles, C.; Van Den Berg, F. G. A.; Gross, L. *Energy Fuels* **2017**, *31*, 6856−6861.

(23) Schuler, B.; Meyer, G.; Peña, D.; Mullins, O. C.; Gross, L. *J. Am. Chem. Soc.* **2015**, *137* (31), 9870−9876.

(24) Sabbah, H.; Morrow, A. L.; Pomerantz, A. E.; Zare, R. N. *Energy Fuels* **2011**, *25* (4), 1597−1604.

DOI: 10.1021/acs.energyfuels.8b01765
Energy Fuels 2018, 32, 9106−9120

(25) Wang, W.; Taylor, C.; Hu, H.; Humphries, K. L.; Jaini, A.; Kitimet, M.; Scott, T.; Stewart, Z.; Ulep, K. J.; Houck, S.; Luxon, A.; Zhang, B.; Miller, B.; Parish, C. A.; Pomerantz, A. E.; Mullins, O. C.; Zare, R. N. *Energy Fuels* **2017**, *31* (9), 9140−9151.
(26) Sabbah, H.; Morrow, A. L.; Pomerantz, A. E.; Mullins, O. C.; Tan, X.; Gray, M. R.; Azyat, K.; Tykwinski, R. R.; Zare, R. N. *Energy Fuels* **2010**, *24* (6), 3589−3594.
(27) Savage, P. E.; Klein, M. T.; Kukes, S. G. *ACS Div. Fuel Chem. Prepr.* **1985**, *30* (3), 408−419.
(28) Yasar, M.; Trauth, D. M.; Klein, M. T. *Energy Fuels* **2001**, *15* (3), 504−509.
(29) Savage, P. E.; Klein, M. T.; Kukes, S. G. *Energy Fuels* **1988**, *2* (12), 619−628.
(30) Trejo, F.; Ancheyta, J.; Mexicano, I.; La, E. C. *Ind. Eng. Chem. Res.* **2007**, *46*, 7571−7579.
(31) Ancheyta, J.; Trejo, F.; Rana, M. S. *Asphaltene Chemical Transformation during Hydroprocessing of Heavy Oils*; CRC Press, Taylor & Francis Group: Boca Raton, FL, 2010; pp 1−86.
(32) Rüger, C. P.; Grimmer, C.; Sklorz, M.; Neumann, A.; Streibel, T.; Zimmermann, R. *Energy Fuels* **2018**, *32*, 2699.
(33) Karimi, A.; Qian, K.; Olmstead, W. N.; Freund, H.; Yung, C.; Gray, M. R. *Energy Fuels* **2011**, *25* (8), 3581−3589.
(34) Strausz, O. P.; Mojelsky, T. W.; Faraji, F.; Lown, E. M.; Peng, P. *Energy Fuels* **1999**, *13* (2), 207−227.
(35) Pomerantz, A. E.; Wu, Q.; Mullins, O. C.; Zare, R. N. *Energy Fuels* **2015**, *29* (5), 2833−2842.
(36) Pinkston, D. S.; Duan, P.; Gallardo, V. A.; Habicht, S. C.; Tan, X.; Qian, K.; Gray, M.; Mullen, K.; Kenttämaa, H. I. *Energy Fuels* **2009**, *23* (11), 5564−5570.
(37) Hurt, M. R.; Borton, D. J.; Choi, H. J.; Kenttämaa, H. I. *Energy Fuels* **2013**, *27* (7), 3653−3658.
(38) Groenzin, H.; Mullins, O. C. *Asphaltenes, Heavy Oils, and Petroleomics*; Springer: New York, 2007; pp 17−60.
(39) Schuler, B.; Zhang, Y.; Collazos, S.; Fatayer, S.; Meyer, G.; Pérez, D.; Guitián, E.; Harper, M. R.; Kushnerick, J. D.; Peña, D.; Gross, L. *Chem. Sci.* **2017**, *8* (3), 2315−2320.
(40) Alvarez, E.; Marroquín, G.; Trejo, F.; Centeno, G.; Ancheyta, J.; Díaz, J. A. I. *Fuel* **2011**, *90* (12), 3602−3607.
(41) Rueda-Velásquez, R. I.; Freund, H.; Qian, K.; Olmstead, W. N.; Gray, M. R. *Energy Fuels* **2013**, *27*, 1817−1829.
(42) Savage, P. E.; Klein, M. T.; Kukes, S. G. *Ind. Eng. Chem. Process Des. Dev.* **1985**, *24* (4), 1169−1174.
(43) Yasar, M.; Trauth, D. M.; Klein, M. T. *Energy Fuels* **2001**, *15* (3), 504−509.
(44) Rubinstein, I.; Spyckerelle, C.; Strausz, O. P. *Geochim. Cosmochim. Acta* **1979**, *43*, 1−6.
(45) Gray, M. R. *Energy Fuels* **2003**, *17* (6), 1566−1569.
(46) Chacón-Patiño, M. L.; Rowland, S. M.; Rodgers, R. P. *Energy Fuels* **2017**, *31* (12), 13509−13518.
(47) Chacón-Patiño, M. L.; Rowland, S. M.; Rodgers, R. P. *Energy Fuels* **2018**, *32* (1), 314−328.
(48) McKenna, A. M.; Marshall, A. G.; Rodgers, R. P. *Energy Fuels* **2013**, *27*, 1257−1267.
(49) Gawrys, K. L.; Blankenship, G.; Kilpatrick, P. K. *Energy Fuels* **2006**, *20* (2), 705−714.
(50) Spiecker, P. M.; Gawrys, K. L.; Kilpatrick, P. K. *J. Colloid Interface Sci.* **2003**, *267* (1), 178−193.
(51) Nyadong, L.; Lai, J.; Thompsen, C.; LaFrancois, C. J.; Cai, X.; Song, C.; Wang, J.; Wang, W. *Energy Fuels* **2018**, *32* (1), 294−305.
(52) Tachon, N.; Jahouh, F.; Delmas, M.; Banoub, J. H. *Rapid Commun. Mass Spectrom.* **2011**, *25* (18), 2657−2671.
(53) Qian, K.; Edwards, K. E.; Mennito, A. S.; Freund, H.; Saeger, R. B.; Hickey, K. J.; Francisco, M. A.; Yung, C.; Chawla, B.; Wu, C.; Kushnerick, J. D.; Olmstead, W. N. *Anal. Chem.* **2012**, *84* (10), 4544−4551.
(54) Riedeman, J. S.; Kadasala, N. R.; Wei, A.; Kenttämaa, H. I. *Energy Fuels* **2016**, *30* (2), 805−809.
(55) Dong, X.; Lu, X.; Romanczyk, M.; Zhang, Y.; Kenttämaa, H. *66th ASMS Conference on Mass Spectrometry and Allied Topics*, San Antonio, TX, USA. June 5−9, 2016.
(56) Alvarez-Ramírez, F.; Ruiz-Morales, Y. *Energy Fuels* **2013**, *27* (4), 1791−1808.
(57) Andrews, A. B.; Edwards, J. C.; Pomerantz, A. E.; Mullins, O. C.; Nordlund, D.; Norinaga, K. *Energy Fuels* **2011**, *25* (7), 3068−3076.
(58) Strausz, O. P.; Mojelsky, T. W.; Faraji, F.; Lown, E. M.; Peng, P. *Energy Fuels* **1999**, *13* (1), 207−227.
(59) Peng, P.; Morales-Izquierdo, A.; Hogg, A.; Strausz, O. P. *Energy Fuels* **1997**, *11* (6), 1171−1187.
(60) Sheremata, J. M.; Gray, M. R.; Dettman, H. D.; McCaffrey, W. C. *Energy Fuels* **2004**, *18* (5), 1377−1384.
(61) Payzant, J. D.; Lown, E. M.; Strausz, O. P. *Energy Fuels* **1991**, *5* (3), 445−453.
(62) Juyal, P.; McKenna, A. M.; Fan, T.; Cao, T.; Rueda-Velásquez, R. I.; Fitzsimmons, J. E.; Yen, A.; Rodgers, R. P.; Wang, J.; Buckley, J. S.; Gray, M. R.; Allenson, S. J.; Creek, J. *Energy Fuels* **2013**, *27* (4), 1899−1908.
(63) Chacón-Patiño, M. L.; Vesga-Martínez, S. J.; Blanco-Tirado, C.; Orrego-Ruiz, J. A.; Gómez-Escudero, A.; Combariza, M. Y. *Energy Fuels* **2016**, *30* (6), 4550−4561.
(64) Kaiser, N. K.; Quinn, J. P.; Blakney, G. T.; Hendrickson, C. L.; Marshall, A. G. *J. Am. Soc. Mass Spectrom.* **2011**, *22* (8), 1343−1351.
(65) Beu, S. C.; Blakney, G. T.; Quinn, J. P.; Hendrickson, C. L.; Marshall, A. G. *Anal. Chem.* **2004**, *76* (19), 5756−5761.
(66) Corilo, Y. E. *PetroOrg Software*; Florida State University, 2013; http://www.petroorg.com.
(67) Galarraga, C. E.; Pereira-Almao, P. *Energy Fuels* **2010**, *24* (4), 2383−2389.
(68) Giraldo-Dávila, D.; Chacón-Patiño, M. L.; McKenna, A. M.; Blanco-Tirado, C.; Combariza, M. Y. *Energy Fuels* **2018**, *32*, 2769.
(69) Purcell, J. M.; Merdrignac, I.; Rodgers, R. P.; Marshall, A. G.; Gauthier, T.; Guibard, I. *Energy Fuels* **2010**, *24* (4), 2257−2265.
(70) Chacón-Patiño, M. L.; Blanco-Tirado, C.; Orrego-Ruiz, J. A.; Gómez-Escudero, A.; Combariza, M. Y. *Energy Fuels* **2015**, *29* (10), 6330−6341.
(71) Pereira, T. M. C.; Vanini, G.; Tose, L. V.; Cardoso, F. M. R.; Fleming, F. P.; Rosa, P. T. V.; Thompson, C. J.; Castro, E. V. R.; Vaz, B. G.; Romão, W. *Fuel* **2014**, *131* (April), 49−58.
(72) Ancheyta, J.; Centeno, G.; Trejo, F.; Marroquín, G.; García, J. A.; Tenorio, E.; Torres, A. *Energy Fuels* **2002**, *16* (5), 1121−1127.
(73) Buenrostro-Gonzalez, E.; Groenzin, H.; Lira-Galeana, C.; Mullins, O. C. *Energy Fuels* **2001**, *15* (13), 972−978.
(74) Liao, Z.; Zhao, J.; Creux, P.; Yang, C. *Energy Fuels* **2009**, *23* (12), 6272−6274.
(75) Boduszynski, M. M. *Energy Fuels* **1987**, *1* (1), 2−11.
(76) Boduszynski, M. M. *Chemistry of Asphaltenes*; American Chemical Society: Washington, DC, 1982; pp 119−135.
(77) Chacón-Patiño, M. L.; Rowland, S. M.; Rodgers, R. P. In *The Boduszynski Continuum: Contributions to the Understanding of the Molecular Composition of Petroleum*; Ovalles, C., Moir, M. E., Eds.; ACS Symposium Series; American Chemical Society: Washington, DC, 2018; Vol. *1282*, pp 113−171.
(78) Groenzin, H.; Mullins, O. C. *Energy Fuels* **2000**, *14*, 677−684.
(79) Badre, S.; Goncalves, C. C.; Norinaga, K.; Gustavson, G.; Mullins, O. C. *Fuel* **2006**, *85* (1), 1−11.
(80) McKenna, A. M.; Purcell, J. M.; Rodgers, R. P.; Marshall, A. G. *Energy Fuels* **2010**, *24* (5), 2929−2938.
(81) McKenna, A. M.; Blakney, G. T.; Xian, F.; Glaser, P. B.; Rodgers, R. P.; Marshall, A. G. *Energy Fuels* **2010**, *24* (5), 2939−2946.
(82) Boduszynski, M. M. *Energy Fuels* **1987**, *1* (1), 2−11.
(83) Adams, J. J. *Energy Fuels* **2014**, *28* (5), 2831−2856.
(84) Cho, Y.; Na, J.; Nho, N.; Kim, S.; Kim, S. *Energy Fuels* **2012**, *26*, 2558−2565.
(85) Gaspar, A.; Zellermann, E.; Lababidi, S.; Reece, J.; Schrader, W. *Energy Fuels* **2012**, *26*, 3481−3487.
(86) Giraldo-Dávila, D.; Chacón-Patiño, M. L.; Orrego-Ruiz, J. A.; Blanco-Tirado, C.; Combariza, M. Y. *Fuel* **2016**, *185*, 45−58.

DOI: 10.1021/acs.energyfuels.8b01765
Energy Fuels 2018, 32, 9106−9120

(87) Rogel, E.; Witt, M. *Energy Fuels* **2017**, *31* (4), 3409−3416.
(88) Rogel, E.; Moir, M. *Fuel* **2017**, *208*, 271−280.
(89) Pinho, B.; Minsariya, K.; Yen, A.; Joshi, N.; Hartman, R. L. *Energy Fuels* **2017**, *31* (11), 11640−11650.
(90) Kaminski, T. J.; Fogler, H. S.; Wolf, N.; Wattana, P.; Mairal, A. *Energy Fuels* **2000**, *14* (1), 25−30.
(91) Wang, S.; Liu, Q.; Xu, C.; Gray, M. *Petrophase 17th International Conference on Petroleum Phase Behavior and Fouling*, Elsinore, Denmark, June 19−23, 2016; p 134.
(92) Fan, Y.; Simon, S.; Sjöblom, J. *Colloids Surf., A* **2010**, *366* (1−3), 120−128.
(93) Yang, X.; Verruto, V. J.; Kilpatrick, P. K. *Energy Fuels* **2007**, *21* (3), 1343−1349.
(94) Sauerer, B.; Stukan, M.; Buiting, J.; Abdallah, W.; Andersen, S. *Langmuir* **2018**, *34* (19), 5558−5573.
(95) Spiecker, P. M.; Kilpatrick, P. K. *Langmuir* **2004**, *20* (10), 4022−4032.
(96) McKenna, A. M.; Purcell, J. M.; Rodgers, R. P.; Marshall, A. G. *Energy Fuels* **2009**, *23* (4), 2122−2128.
(97) Cho, Y.; Kim, Y. H.; Kim, S. *Anal. Chem.* **2011**, *83* (15), 6068−6073.
(98) Islam, A.; Cho, Y.; Ahmed, A.; Kim, S. *Mass Spectrom. Lett.* **2012**, *3* (3), 63−67.
(99) Pereira, T. M. C.; Vanini, G.; Oliveira, E. C. S.; Cardoso, F. M. R.; Fleming, F. P.; Neto, A. C.; Lacerda, V.; Castro, E. V. R.; Vaz, B. G.; Romão, W. *Fuel* **2014**, *118*, 348−357.
(100) Hsu, C. S.; Lobodin, V. V.; Rodgers, R. P.; McKenna, A. M.; Marshall, A. G. *Energy Fuels* **2011**, *25*, 2174−2178.
(101) Lobodin, V. V.; Marshall, A. G.; Hsu, C. S. *Anal. Chem.* **2012**, *84*, 3410−3416.
(102) Blanco-Tirado, C.; Combariza, M. Y.; Blanco-Combariza, C. A. *66th ASMS Conference on Mass Spectrometry and Allied Topics*, Indianapolis, IN, 2017.
(103) Dias, J. R. *J. Chem. Inf. Comput. Sci.* **1999**, *39*, 197−203.
(104) Dias, J. R. *J. Phys. Chem. A* **1997**, *101*, 7167−7175.
(105) Ruiz-Morales, Y. *J. Phys. Chem. A* **2002**, *106* (46), 11283−11308.

DOI: 10.1021/acs.energyfuels.8b01765
Energy Fuels 2018, 32, 9106−9120